Earth, Planets and Space

FULL PAPER Open Access

Aftershock analysis and forecasting for the crustal seismicity in Romania

Cristian Ghita[1], Bogdan Enescu[1,2*], Alexandru Marinus[1], Iren-Adelina Moldovan[1], Constantin Ionescu[1], Eduard Gabriel Constantinescu[1] and Like An[2]

Abstract

Romania is known for its persistent seismicity at intermediate-depths in the Vrancea region. However, crustal areas are also a significant source of seismic hazard, although large shallow events are less common. This study is a first attempt to characterize statistically and propose a forecasting model for two recent aftershock sequences occurred at crustal depths in 2014 and 2023, following mainshocks of moderate magnitudes (M_w5.4 for both mainshocks). We apply a robust approach based on a state-of-the-art procedure developed and tested previously for Japan, which is able to determine in quasi real-time the parameters of the Gutenberg–Richter law and Omori–Utsu law for aftershocks and provide probability estimates of larger events, which can be updated in real time. For both the 2014 Vrancea-Marasesti and 2023 Gorj-Oltenia sequences we test several relatively short (hours to one day) learning periods and subsequent forecasting periods. Both sequences are characterized by a Gutenberg–Richter *b*-value around 0.8–0.9, which is only slightly lower than the average of 1.0 for worldwide seismicity. The aftershock decay is characterized by a parameter *p* of around 1.0, commonly observed for crustal aftershock sequences. The *c*-value, which indicates the onset time of the power-law decay of aftershocks, is on the order of minutes to hours. Although the two studied sequences follow mainshocks having the same moment magnitude, the probability of larger aftershocks for the 2023 Gorj-Oltenia sequence are larger. The results obtained in this study are encouraging for the development of a real-time monitoring and forecasting system for the Romanian crustal seismicity.

Keywords Real-time aftershock forecasting, Seismic sequences, Crustal seismicity, Romania

*Correspondence:
Bogdan Enescu
benescu@kugi.kyoto-u.ac.jp
Full list of author information is available at the end of the article

Graphical Abstract

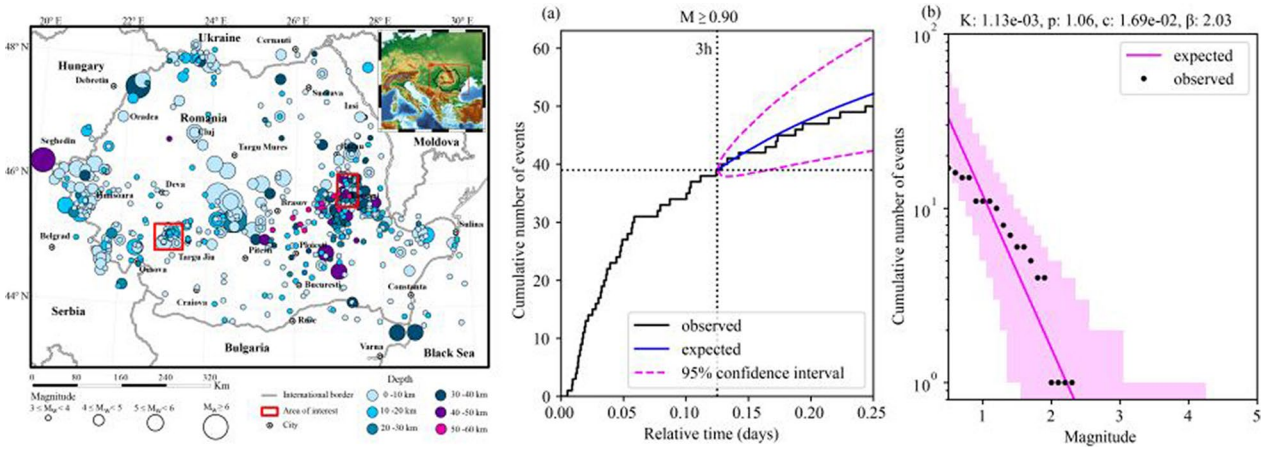

1 Introduction

1.1 A brief overview of seismicity forecasting and challenges

Studying the space–time evolution of earthquake sequences is of importance for understanding their underlying physical processes, like migration of fluids and slow slip (e.g., Shimojo et al. 2021) within the seismogenic zone, as well as for seismic hazard mitigation. The importance of reducing damages and losses after larger mainshocks supports the efforts being made to develop dedicated aftershock forecasting tools. Statistical methods based on the frequency–magnitude distribution of earthquakes (Gutenberg and Richter 1944) and aftershock frequency decay with time from the mainshock (e.g., Utsu 1961) have proven effective in forecasting seismicity (e.g., Reasenberg and Jones 1989; Page et al. 2016; Omi et al. 2019).

In general, aftershock forecasts are given based on the data that are revised and prepared at the time of a study or the data transmitted in real-time into a semi-automatic system. The latter type is more likely to experience forecasting accuracy problems, due to a higher predisposition to errors. These errors may include a lack or reduced number of recording seismic stations in the study area, seismic sensor malfunctioning, overlapping earthquakes on seismograms for certain time periods, especially at short times following a mainshock, miscalculated magnitudes, and errors of epicenter determination (e.g., Omi et al. 2016 and references therein). Addressing such challenges is difficult, however the scientific and societal importance of aftershock forecasting encourages the development of new approaches and the refinement of older ones.

Many studies in the recent years focus on forecasting seismic activity (for a review, we refer to Mizrahi et al. 2024a, b), aftershocks in particular (Hardebeck et al. 2024). Broadly speaking, there are two classes of models: physics-based forecasting models that are primarily following the time evolution of certain physical parameters (e.g., static stress changes) and attempt to forecast future seismicity based on empirical relations (e.g., the rate-and-state friction law) between these parameters and earthquake rates (e.g., Toda and Enescu 2011; Cattania et al. 2018; Jia 2020; Feng et al. 2022; Dahm and Hainzl 2022) and statistical models that are based primarily on the stochastic nature of seismic activity and, in many cases, employ an ETAS-type seismicity model (Zhuang 2011; Nandan et al. 2019; Mancini et al. 2022; Savran et al. 2020; van der Elst et al. 2022; Mizrahi et al. 2024a, b; Petrillo and Zhuang 2024). While the ETAS models are the current state-of-art standard of analyzing and forecasting seismicity, we have adopted in this work the simpler, but nevertheless robust approach developed in a series of works by Omi and collaborators, which is currently in use for forecasting aftershock occurrence in Japan and implemented at the National Research Institute for Earth Science and Disaster Resilience (NIED) (e.g., Omi et al. 2019).

One of the challenges when analyzing and forecasting seismicity is the proper estimation of the magnitude of completeness of the data. Numerous studies have been dedicated to this issue; many of the developed methods are based on the curvature of the supposedly linear frequency–magnitude (frequency in log scale) distribution of earthquakes or on quantifying deviations from the linear trend (for a review, see Mignan and Woessner 2012).

The method proposed by Ogata and Katsura (1993) models the entire magnitude range of the earthquake data by considering the observed frequency–magnitude distribution as the product of an exponential distribution (i.e., the Gutenberg–Richter (1944) distribution) and a detection probability function (detailed explanations are given in the Methods section). The estimation of the correct magnitude of completeness is particularly important since it impacts the determined *b*-value of the frequency–magnitude distribution of earthquakes (e.g., Mignan and Woessner 2012). Newly developed approaches for *b*-value determination (e.g., van der Elst 2021; Lippiello and Petrillo 2024) have been shown to be particularly robust to data incompleteness issues. The current research is based on the determination of the *b*-value according to the method proposed by Ogata and Katsura (1993). Nevertheless, we compare β-values (proxies for *b*-values—see the Methods section for parameter definition) obtained using the so-called *b*-positive method (van der Elst 2021) to the ones determined based on our forecasting workflow.

1.2 Seismicity of Romania and purpose of current study

Romania has both crustal and subcrustal seismicity. The Vrancea region (Romania) is well-known for its energetic subcrustal, intermediate-depth seismicity (e.g., Enescu et al. 2023; Petrescu and Enescu 2025), with the largest events having magnitudes above 7.0, like the destructive March 4, 1977 M_w7.5 earthquake (e.g., Fuchs et al. 1979). The crustal events in Romania (Fig. 1) are less energetic and less persistent compared to the Vrancea subcrustal earthquakes, being typically classified as moderate seismic swarms and foreshock–mainshock–aftershock sequences (Popescu and Radulian 2001; Popescu et al. 2011, 2012). Due to their relatively shallow hypocentral locations, these crustal earthquakes pose a considerable seismic hazard (e.g., Moldovan et al. 2008; Pavel 2017).

In the last decade, the National Seismic Network of Romania has benefited from an increasing number of seismic stations, which led to a significant increase in the number of earthquakes detected and located on the territory of Romania and neighboring regions (Marmureanu et al. 2021), as recorded in the ROMPLUS seismic catalog (e.g., Oncescu et al. 1999; Popa et al. 2015, 2022), prepared and provided by the National Institute for Earth Physics (NIEP).

The purpose of this study is twofold. First, we focus on the statistical analysis of two crustal seismic sequences associated with the largest recent events that occurred in the recent years on the Romanian territory, in the Vrancea-Marasesti area and Gorj-Oltenia region, respectively (Fig. 1). The mainshocks in both regions had a moment magnitude M_w5.4 and occurred at crustal depths, as described in detail in the next section. A related purpose of this study is the forecasting of the aftershock activity in the two regions and the development of an aftershock forecasting system that would be the first of its kind for the territory of Romania. The presented system for automated aftershock forecasting in Romania targets generating results from the first few hours to the first few days after a mainshock, using previously proposed statistical techniques that have been applied successfully to the seismicity of Japan (Omi et al. 2013, 2014, 2015, 2016, 2019).

1.3 Earthquake data for the Marasesti and Gorj earthquake sequences

One of the largest crustal events, M_W5.4 (M_L5.7) instrumentally recorded in Romania occurred in the Vrancea-Marasesti (referred from now on as Marasesti) area (Fig. 2a), at a depth $Z=40.9$ km, on November 22, 2014, at 21:14 (Ghita et al. 2021) and was followed by an aftershock sequence consisting of 222 recorded earthquakes, with $M_L \geq 0.1$, that spanned a period of about 70 days from the mainshock. The sequence occurred in the Focsani basin, part of the Moesian Platform (a major structural unit of the Carpathian and Balkans foreland, e.g., Seghedi et al. 2005), and is related to the normal fault system associated to the major Peceneaga-Camena fault, which separates the Moesian Platform from the North Dobrogea promontory (Craiu et al. 2019).

Another intense earthquake sequence occurred on February 2023 in the Gorj area (Oltenia province), northwest of Targu Jiu city (Fig. 2b), situated in the northwestern part of Central-South Carpathian zone (Oros et al. 2023), at the contact between the Getic Depression, to the South, and the Southern Carpathians orogen, to the North. The Gorj-Oltenia sequence (referred from now as the Gorj sequence) started with a magnitude M_W4.8 (M_L5.2) at a depth $Z=18.3$ km foreshock on February 13, 2023, at 16:58:09, followed by the M_W5.4 (M_L5.7) mainshock on February 14, 2023, at 15:16:52, the largest earthquake ever recorded or reported in the area, at a depth $Z=14$ km (we note here that the larger earthquake in the sequence can also be considered an aftershock of the former, but we adopt here the foreshock–mainshock definition). Apart from this seismic event, the second largest magnitude (M_W5.2) earthquake occurred in this area is the one from northwest of Targu Jiu, at a depth of 9.9 km, on June 20, 1943. It is worth noting that another sequence was recorded in the study area in 2011–2012 (Radulian et al. 2014), with smaller magnitude earthquakes (maximum magnitude of M_W3.8), which occurred on reverse faults located eastward from the current sequence (Fig. 1).

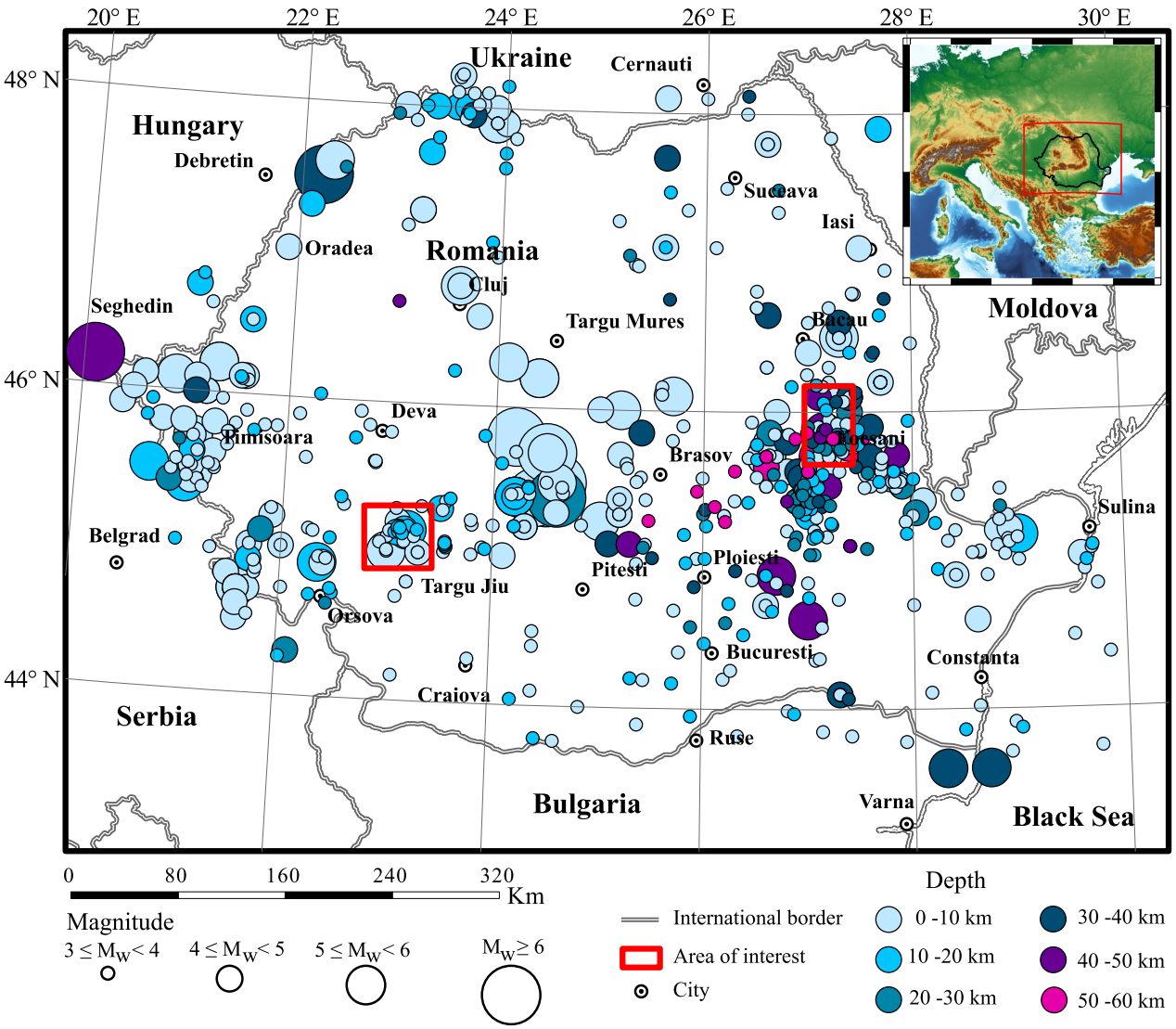

Fig. 1 Seismicity of Romania, earthquakes of $M_W > 3.0$, depths smaller or equal to 60 km (i.e., the intermediate-depth Vrancea seismicity, with depth from 60 to 180 km is excluded). Red rectangles mark the Marasesti (to the east) and Gorj (to the south-west) areas, where the studied earthquake sequences occurred. The period of the ROMPLUS catalog spans from 12.05.1022 to 26.10.2023. The inset shows the positioning of Romania within a larger geographic region

Starting February 22, 2023, due to the installation of three mobile seismic stations in the Gorj epicentral zone: BVPR, CPSR, DBRR (Fig. 2b), a better location of the aftershocks was achieved, together with the decrease of the magnitude of completeness in the area.

For the analysis, we used the real-time data-portal earthquake catalog (https://dataportal.infp.ro) and the ROMPLUS earthquake catalog (Oncescu et al. 1999) for the Gorj and Marasesti areas, respectively. Our analysis and forecasts are based on the early stages of aftershocks sequences. The real-time system component of the data-portal is based on the Antelope data acquisition and processing software for handling large amounts of real-time recorded data (Popa et al. 2015). Because the data-portal real-time catalog has the magnitudes given in M_L, from now on, in our study we will use only the M_L magnitude. Local time is used throughout the study. The forecasting parameters for the Marasesti area were estimated using seismic events from the ROMPLUS catalog (Oncescu et al. 1999; Popa et al. 2015, 2022), between November 22, 2014, at 21:14, and February 1, 2015, at 23:31. ROMPLUS has been used since the data-portal was not fully developed at the time of the sequence. The Gorj area dataset

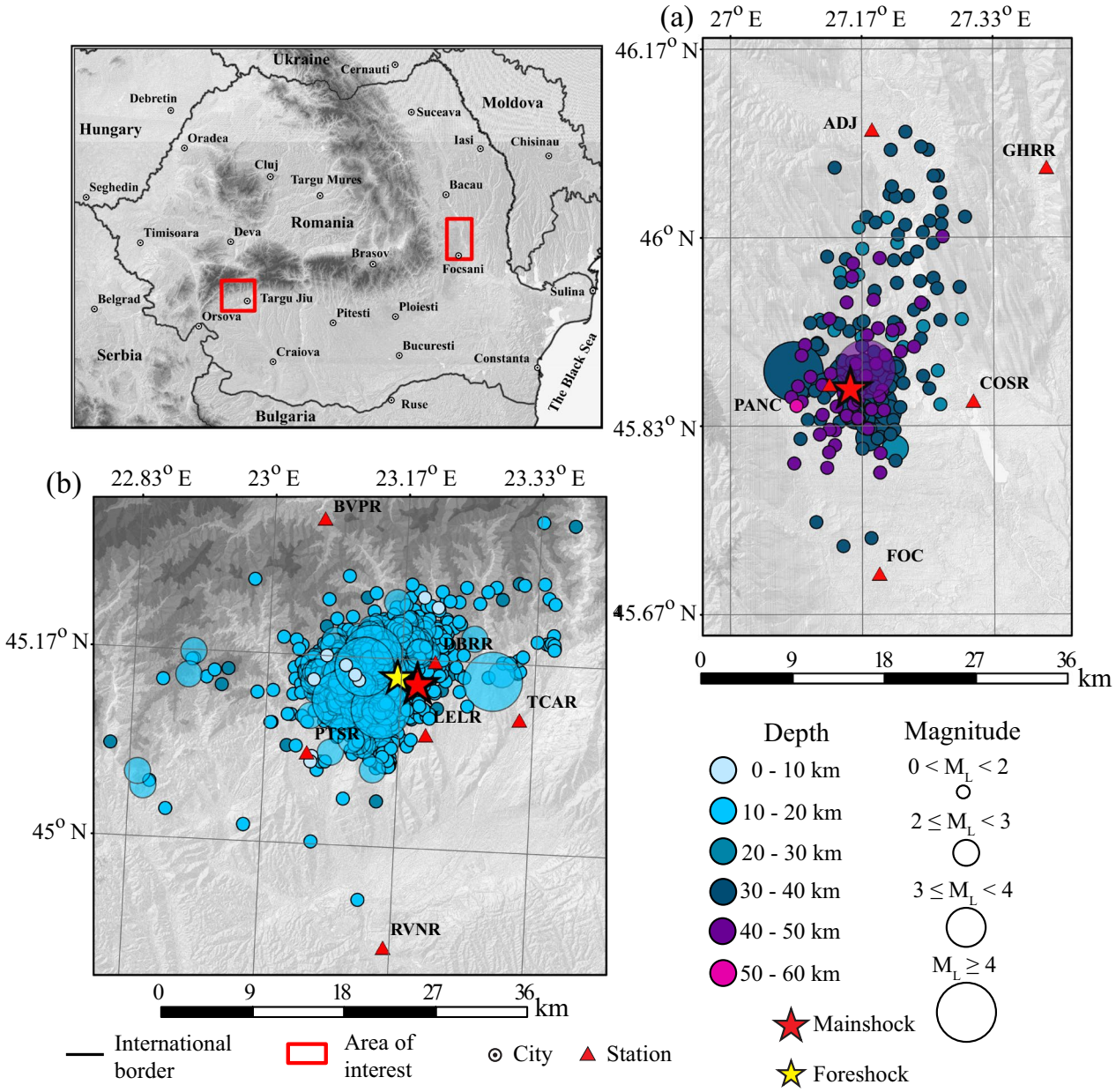

Fig. 2 Seismic sequences analyzed in this study. The map in **a** shows the seismic sequence recorded at Marasesti, with a mainshock of M_W 5.4, occurred on November 22, 2014, while **b** shows the seismic sequence recorded at Gorj, with a mainshock of M_W 5.4, occurred on February 14, 2023. Upper left inset shows a map of Romania, with the two studied regions indicated by rectangles

contains the location parameters and magnitudes of the foreshock, mainshock and other 2175 earthquakes with $M_L \geq 1.2$ recorded from February 13, 2023, at 14:58:09 to March 24, 2023, at 4:02, as retrieved from the data portal.

For the Marasesti sequence (Fig. 2a), we refer to the crustal events with depth $18 \leq Z \leq 50.0$ km, and magnitudes $0.1 \leq M_L \leq 5.7$, recorded from 22 November 2014 to February 1, 2015, in the area bordered by 45.67°N–46.17°N latitude and 26.83°E–27.5°E longitude (Fig. 2a) (Ghita et al. 2021). The depth range has been chosen based on the depth range of crustal seismicity in this area, for longer periods of time.

For the Gorj sequence (Fig. 2b), we refer to the crustal events with depth $1.0 \leq Z \leq 27$ km (chosen based on the depth of the seismogenic area), and magnitudes $0.1 \leq M_L \leq 5.7$, recorded from February 14, 2023, to March 20, 2023, in the area bordered by 44.93°N–45.27°N

latitude and 22.80°E–23.40°E longitude (Fig. 2b), with a large potential of significant regional earthquake activity, as documented in previous studies (Placinta et al. 2016; Ghita et al. 2020). In the last years, studies of Bala et al. (2020) and Oros et al. (2023) have referred to the earthquakes in this area as belonging to a crustal seismogenic source named Central-South Carpathians (CSCSZ).

2 Methods

In the present study we estimate the Omori–Utsu law and Gutenberg–Richter law (see below for their definition) parameters for the two earthquake sequences introduced in the previous sub-section, using various time periods as learning periods, and forecast the aftershock activity for periods that follow the learning periods. The approach used in this paper follows closely that proposed by Omi et al. (2013, 2019).

The Omori–Utsu law (Utsu 1961; Utsu et al. 1995) is an empirical relation that describes the decay of the aftershock rate following a mainshock, according to a non-stationary Poisson process, as expressed by the formula:

$$\mathrm{N(t)} = \frac{\mathrm{K}}{(\mathrm{t}+\mathrm{c})^{\mathrm{p}}}, \tag{1}$$

where $N(t)$ represents the aftershock rate function of the time t (in days) after the mainshock, while K, c and p are parameters dependent on the earthquake sequence. The parameter K is a constant that sets the scale of the aftershock sequence (i.e., describes the productivity of the sequence), c is the time delay before the onset of the power-law decay of aftershock activity with a slope given by the parameter p, representing how fast the aftershock activity is decaying with time, t, from the mainshock.

The Gutenberg–Richter law (Gutenberg and Richter 1944), which expresses the frequency–magnitude distribution (FMD) of earthquakes, can be defined as:

$$\mathrm{m(M)} = \mathrm{A} \times 10^{-bM} \propto \exp(-\beta M), \tag{2}$$

where $m(M)$ is the frequency of earthquakes (normalized number of events) of magnitude M and A and b (or $\beta = b^{*}ln10$) are constants. In a statistical framework, $m(M)$ is the intensity of events with magnitude M.

The joint occurrence rate of aftershocks, λ, as a function of time from the mainshock, t, and magnitude M is represented by the product of $N(t)$ and $m(M)$. So, by combining $N(t)$ and $m(M)$ we get:

$$\lambda(\mathrm{t},\ \mathrm{M}) = \frac{K'}{(t+c)^{p}}\beta e^{-\beta(M-M_0)}, \tag{3}$$

where $K' = \beta^{-1}KA \exp(-\beta M_0)$, and M_0 is the magnitude of the mainshock used to adjust the scale of K' (Utsu 1970). Hereafter, to simply notations, we use K instead of K' (e.g., Morikawa et al. 2021).

Note that the occurrence rate of aftershocks for earthquakes with magnitudes equal or larger than a threshold magnitude M_t can be obtained by integrating (3) as follows:

$$\lambda(\mathrm{t}) = \int_{M_t}^{\infty} \lambda(t, M)\mathrm{d}M. \tag{4}$$

Many small aftershocks are incompletely recorded in seismic catalogs at early times after the mainshock (e.g., Utsu et al. 1995; Kagan 2004; Peng et al. 2007; Enescu et al. 2009). In order to address the incompleteness issue, the detection rate as a function of magnitude (e.g., Ogata and Katsura 1993; Omi et al. 2013) is used:

$$\phi(\mathrm{M}|\mu,\sigma) = \frac{1}{\sqrt{2\pi\sigma^2}}\int_{-\infty}^{\mathrm{M}} \mathrm{dx}\exp\left[-\frac{(\mathrm{x}-\mu(\mathrm{t}))^2}{2\sigma^2}\right], \tag{5}$$

where μ represents the magnitude with a 50% detection rate and σ represents the scale for a range of magnitudes around m where earthquakes are more or less frequently detected. In order to obtain the "real" frequency–magnitude distribution (i.e., the distribution that would be observed if there were no detection issues), the observed frequency–magnitude distribution $m(M)$ (Eq. 2) is multiplied with the detection rate function $\phi(M|\mu,\sigma)$ (Eq. 4). The parameters β, μ and σ can be simultaneously determined (e.g., Ogata and Katsura 2006) by fitting the magnitude data of all detected earthquakes to a probability density that is the normalized version of $m(M)^{*}\phi(M|\mu,\sigma)$, through a maximum likelihood procedure. Note that the detection rate strongly depends on the elapsed time since the mainshock (e.g., Enescu et al. 2009; Peng and Zhao 2009).

Omi et al. (2013) have developed a state-space model for an objective Bayesian inference of the time-dependent parameter $\mu(t)$ and employed a Gaussian prior probability distribution of the b-value for robust estimation using short data from an early period. Given the estimate of the b-value and detection rate function, one can next estimate the parameters K, c and p of the Omori–Utsu formula for the underlying aftershocks by maximizing a log-likelihood function (for details we refer to Omi et al. 2013).

We can also calculate the expected number of underlying aftershocks, N_t, with magnitudes equal or above a threshold magnitude M_t, for a forecast window spanning from t_1 to t_2, by integrating (4) (Reasenberg and Jones 1989):

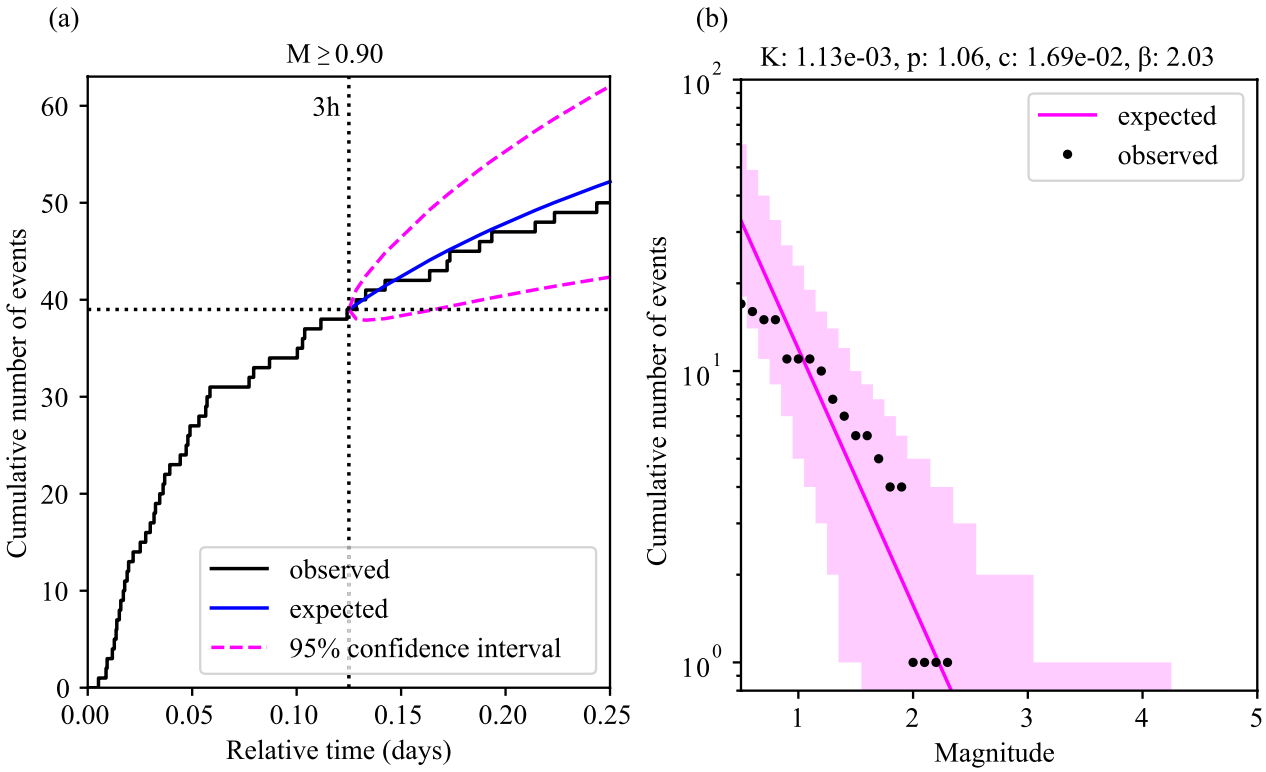

Fig. 3 Analysis of the Marasesti sequence. **a** Aftershock cumulative number (black thick curve) for the learning period [0, 3 h] and forecast period [3 h, 6 h] for the Marasesti area. The expected values for the forecasted period are indicated by the blue curve, together with the 95% confidence interval (dotted magenta). The threshold magnitude (0.9) is taken to be equal with the *Mc* at the end of the learning period (Fig. 4b). **b** The frequency–magnitude distribution for the forecasting window (black—observed numbers, magenta—expected numbers). The Omori–Utsu law parameter values and the β-value estimated during learning are given at the top of the figure

$$N_t = \int_{t_1}^{t_2} \lambda(t)\mathrm{d}t. \tag{6}$$

The probability, P, that at least one aftershock with a magnitude equal or above the M_t threshold occurs in the forecast window (Reasenberg and Jones 1989; Utsu et al. 1995) is given as:

$$P = 1 - \exp(N_t). \tag{7}$$

The probability depends strongly on the model parameters, which are estimated by Reasenberg and Jones (1989) using Bayesian statistics, namely the maximum a posteriori estimate. Here we follow Omi et al. (2019) and use many sets of likely parameter values sampled from the posterior distribution. The approach, referred also as Bayesian forecasting (e.g., Nomura et al. 2011; Omi et al. 2015), provides an ensemble forecast by combining individual forecasts based on the Omori–Utsu (Eq. 1) and Gutenberg–Richter (Eq. 2) models. The range of parameters characterizing these models represent the epistemic uncertainties associated with our earthquake sequences, for the different periods of time. The mean of the individual forecasts is used as the output forecast value.

In our computations, we have chosen M_t as the rounded magnitude of completeness, M_c, for the data at the end of the learning period. This should be in general a reasonable first approximation, since in general the magnitude of completeness decreases with time from the mainshock. M_c can be estimated using the formula:

$$M_C(n) = \mu + n\sigma, \tag{8}$$

where n indicates the confidence level: $n=0$ means that 50% of the events are detected above M_c, while $n=(1, 2, 3)$ means that 68, 95 and 99% of the events are detected (e.g., Mignan and Woessner 2012). In this study we chose $n=2$.

3 Results and discussion

3.1 Parameter estimations and aftershocks' number forecasting for the 2014 Vrancea-Marasesti earthquake sequence

We present first the Omori–Utsu and Gutenberg–Richter laws parameter estimations for the Marasesti earthquake sequence, as well as the aftershock forecasts

Table 1 Summary of parameter estimations for the Vrancea-Marasesti sequence, including their errors, according to the corresponding learning periods

Learning period, related figures and number of events	*K*	*p*	*c [days]*	*β*	*b*
0–3 h (Figs. 3, 4) (65, 22)	1.1×10^{-3} ($\pm 5.71 \times 10^{-3}$)	1.06 (±0.12)	1.69×10^{-2} ($\pm 1.08 \times 10^{-2}$)	2.03 (±0.25)	0.88 (±0.11)
0–6 h (Figs. S1, S2) (87, 18)	1.68×10^{-3} ($\pm 3.11 \times 10^{-3}$)	1.10 (±0.11)	1.58×10^{-2} ($\pm 8.98 \times 10^{-3}$)	1.9 (±0.25)	0.83 (±0.11)
0–9 h (Figs. S3, S4) (96, 19)	2.6×10^{-3} ($\pm 4.17 \times 10^{-3}$)	1.09 (±0.10)	1.67×10^{-2} ($\pm 7.59 \times 10^{-3}$)	1.81 (±0.19)	0.79 (±0.08)
0–12 h (Figs. S5, S6) (105, 17)	3.4×10^{-3} ($\pm 9.95 \times 10^{-3}$)	1.09 (±0.11)	1.71×10^{-2} ($\pm 8.53 \times 10^{-3}$)	1.76 (±0.25)	0.76 (±0.11)
0–24 h (Figs. S7, S8) (122, 22)	4.1×10^{-3} ($\pm 6.5 \times 10^{-3}$)	1.05 (±0.10)	1.69×10^{-2} ($\pm 9.24 \times 10^{-3}$)	1.74 (±0.17)	0.75 (±0.07)

The first column also shows the related figures and the number of events in the learning and forecasting window, respectively

for this sequence. To perform calculations that are meaningful for real-time forecasting, we chose relatively short learning periods of 3 h (Fig. 3), and 6, 9, 12 and 24 h (Additional File 1, Figures S1–S8) after the mainshock. We forecasted the cumulative number of aftershocks for the same number of respective hours following the learning periods.

By using a learning period [0 3 h], containing 65 events, we estimated the following Omori–Utsu law (Eq. 1) parameters: $K = 1.13$*10–3, $c = 0.0169$ and $p = 1.06$ (see also Table 1). The β-value of the Gutenberg–Richter law (Eq. 2) is 2.03.

The b-value calculated from the β-value estimated for the first 3 h of aftershock activity in the area is approximately equal to 0.88, which is slightly lower than the average value of ~1.0, observed for worldwide seismicity (e.g., Godano et al. 2014), indicating a slightly higher proportion of larger aftershocks. The c-value of 0.0169 days indicates that the power-law onset of the aftershock decay starts after approximately 24 min from the mainshock, while the p-value of 1.06 indicates a commonly observed decay rate of aftershocks (e.g., Utsu et al. 1995).

Figure 3a shows the cumulative number of aftershocks for the learning and forecasted windows, as well as expected number of aftershocks during the forecasted period, for aftershocks of magnitudes equal or above a threshold value, M_t, of 0.9 (chosen as the M_c value at the end of the learning period). It can be noticed that the observed aftershock number is within the 95% confidence interval and close to the forecasted aftershock number. The frequency–magnitude distribution during the forecasted period is also in good agreement with the estimations based on the learning period.

Figure 4a presents the scatter plot matrix for the estimated parameter sets, in the case of the Marasesti sequence. Figure 4b shows a slow decrease of the detection magnitude $\mu(t)$ and completeness magnitude, $M_c(t)$, during the 3 h learning period.

The parameter estimations for other learning periods are summarized in Table 1 and, in general, prove to be stable. The forecasted number of aftershocks is in most cases within the estimated 95% confidence limits (Figures S1, S3, S5 and S7). Table 3 summarizes the detection parameters obtained for the considered learning periods. While in general it is expected that $\mu(t)$ and $M_c(t)$ improve with time, one can notice that this may not be the case of the current sequence (Table 3). We speculate that the station coverage at that time in the studied region, the routine detection and location procedures, as well as the dynamics of the sequence, may have impacted the earthquake detection capability evolution with time. As one can notice in Figures S2, S4, S6 and S8, after about 3 h from the start of the sequence there is some slight increase in the number of larger event magnitudes that may cause the increase of $\mu(t)$ and $M_c(t)$ with time. In addition, the sequence might have been characterized by hypocentral expansion predominantly along latitude (not shown since we are not very confident in the location accuracy), which we speculate may have affected the recording and detection capability of earthquakes as a function of time.

The results for the learning period of 6 h, [0 6 h], and forecasted period of [6 h 12 h] are presented in Figures S1 and S2. For the learning period of [0 6 h], the β-value has a small decrease to 1.90, leading to a b-value of approximately 0.83, suggesting that larger

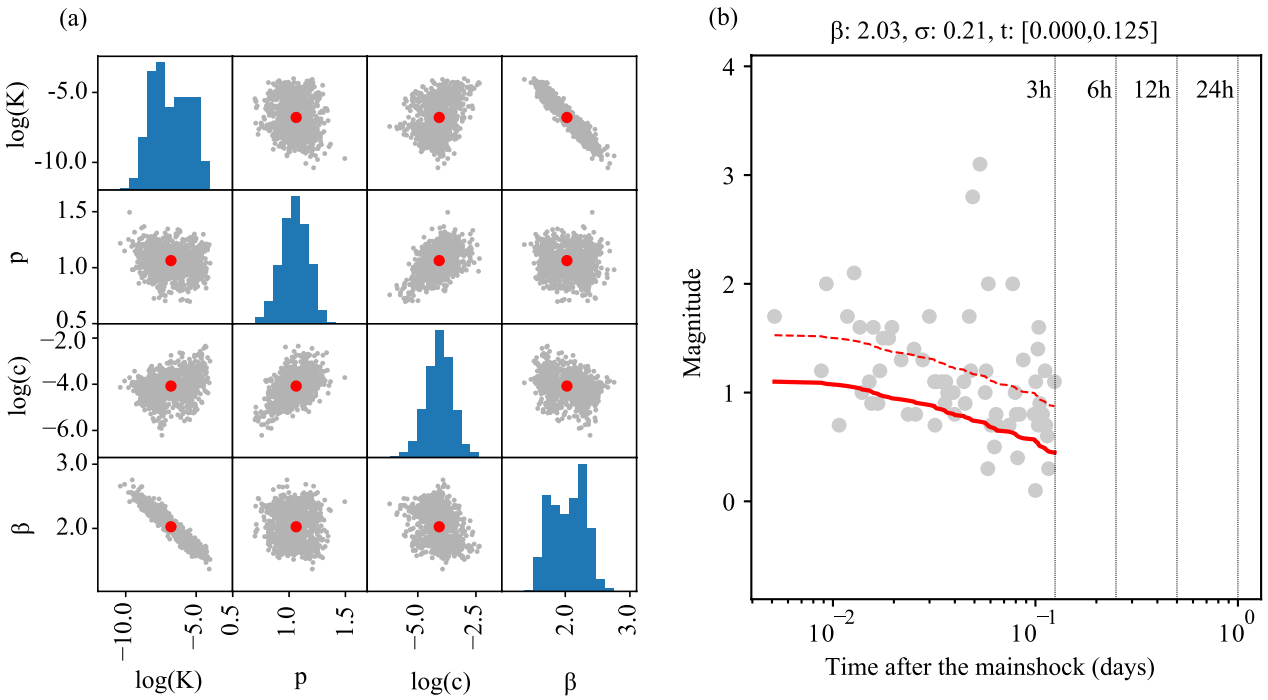

Fig. 4 Estimated parameter sets and evolution of the detection magnitude, $\mu(t)$, and completeness magnitude, $Mc(t)$, for the Marasesti sequence (learning period: [0, 3 h] after the mainshock). **a** Scatter plot distributions for the estimated parameter sets for the Marasesti sequence (red dots: estimated parameters, gray dots: sampled parameter sets). **b** Evolution of $\mu(t)$ (continuous red line) and $Mc(t)$ (dotted red line) during the learning period

aftershocks occur more frequently in the Marasesti area. Like for the previously used learning period [0 3 h], aftershock activity decreases following a power-law with an onset of approximately 23 min from the mainshock ($c=0.0158$ days), at a decay rate, given by $p=1.1$. In addition, for the forecasted period, the difference between the expected and observed cumulative aftershock numbers is within the 95% confidence interval (Figure S1a), while the observed frequency–magnitude distribution is less well predicted by the model (Figure S1b). Figure S2b shows a slow decrease of $\mu(t)$ and $M_c(t)$ magnitudes during the 6 h of the learning period.

The learning period of 9 h from the mainshock is characterized by a β-value of 1.81, equivalent to b-value = 0.79, reconfirming the relatively higher frequency of larger aftershocks for this sequence. The aftershock decay parameters are $c=0.0167$ and $p=1.09$. The expected and observed cumulative number of earthquakes for the forecasted period are relatively close one to each other (Figure S3a), while the observed frequency–magnitude distribution is within the predicted confidence bounds (Figure S3b).

For all tests on the Marasesti sequence, the estimated c-value is relatively small, consistent with well-observed aftershock sequences (e.g., Peng et al. 2007; Enescu et al. 2009) and may reflect early aftershock incompleteness. The p-value is only slightly larger than the average of ~1.0, which indicates typical stress relaxation. The b-value is around 0.8–0.9 (only slightly lower than the average of 1.0), which might hint to higher differential stresses (e.g., Scholz 2015; Tormann et al. 2015). The K-value of the Omori–Utsu law has the same order through all estimations (Table 1), although it slightly increases for later time intervals.

3.2 Parameter estimations and aftershocks' number forecasting for the 2023 Gorj earthquake sequence

The earthquake catalog for the Gorj sequence is retrieved from the data-portal and consists of 2156 events. Among these, 65 aftershocks correspond to the first 3 h of activity after the mainshock and produce a β-value estimation of 2.09, resulting in a b-value approximately equal to 0.91, similar to the β-value and b-value estimations made for the Marasesti sequence. The aftershock activity decreases at a commonly observed decay rate ($p\sim1.0$), from an onset time of about 29 min from the mainshock ($c=0.204$ days) (Fig. 5b). A M_t of 1.9 (determined as the rounded M_c at the end of the learning period) produces an expected cumulative aftershock number that is close to the observed one (Fig. 5a).

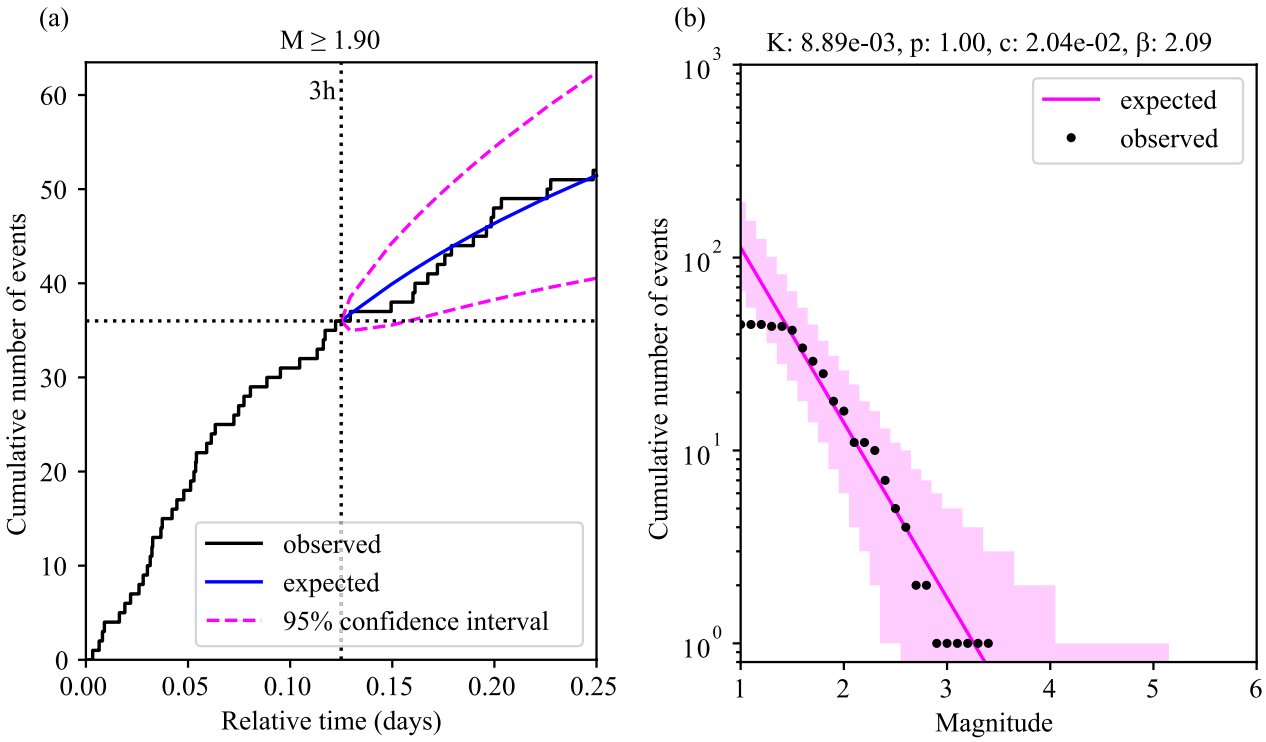

Fig. 5 Analysis of the Gorj sequence. **a** Aftershock cumulative number (black thick curve) for the learning period [0, 3 h] and forecast period [3 h, 6 h] for the Gorj area. The expected values for the forecasted period are indicated by the blue curve, together with the 95% confidence interval (dotted magenta). The threshold magnitude (1.9) is taken to be equal with the *Mc* at the end of the learning period (see Fig. 6b). **b** The frequency–magnitude distribution for the forecasting window (black—observed numbers, magenta—expected numbers). The Omori–Utsu law parameter values and the β-value estimated during the learning period are given at the top of the figure

Figure 6a presents the scatter plot matrix for the estimated parameter sets, in the case of the Gorj sequence. Figure 6b shows a steep decrease of $\mu(t)$ and $M_c(t)$, at the beginning of the 3 h of the learning period, followed by an slightly changing plateau; the rounded M_c reaches a value of 1.9 at the end of the learning period.

In the same way as for the Vrancea-Marasesti sequence, we have made parameter estimations for longer learning periods (Table 2) and forecasted the number of aftershocks for subsequent forecasting periods (Additional File 1—Figures S9–S16).

The learning period [0 6 h] has 108 events and is characterized by a β-value of 2.02 (b-value of 0.88). The aftershock decay is characterized by p-value = 1.0, while the c-value gets slightly larger (c = 0.0806 days (116.1 min)). A M_t of 1.6 produces an expected cumulative aftershock number that is close to the observed one (Figure S9a). Figure S10b shows a slow decrease of $\mu(t)$ and $M_c(t)$ during the 6 h of the learning period.

When analyzing the case of the [0, 9 h] learning period, the number of aftershocks is 143, characterized by a β-value of 1.94 (b-value of 0.84). The aftershock decay is characterized by p = 1.02 and c = 0.0759 (109.3 min). A threshold magnitude of 1.5 produces expected cumulative aftershock numbers that are slighlty lower than the observed ones, but above the lower limit of 95% confidence interval (Figure S11a). Figure S12b shows the $\mu(t)$ and M_c decaying gradually, with M_c reaching a value of 1.5 at the end of the 9 h interval.

Due to catalog incompleteness and the lack of mobile seismic stations until February 22, 2023, the productivity, K-value, for the Gorj sequence presents a relatively large variation when comparing the values for the 12-h and 24-h learning periods. In addition, the b-value is overall slightly larger than for the Marasesti area. The p-values estimated for all learning periods are around 1.0 and c-values are on the same order as for the Marasesti sequence. The results are relatively robust relative to the choice of the learning period and the forecasted number of earthquakes are in general within the estimated confidence values for the forecasting periods. Values utilized for the threshold magnitude are presented in Table 3. Note that with the exception of the last learning period of 24 h, M_c is decreasing at the end of the longer learning periods.

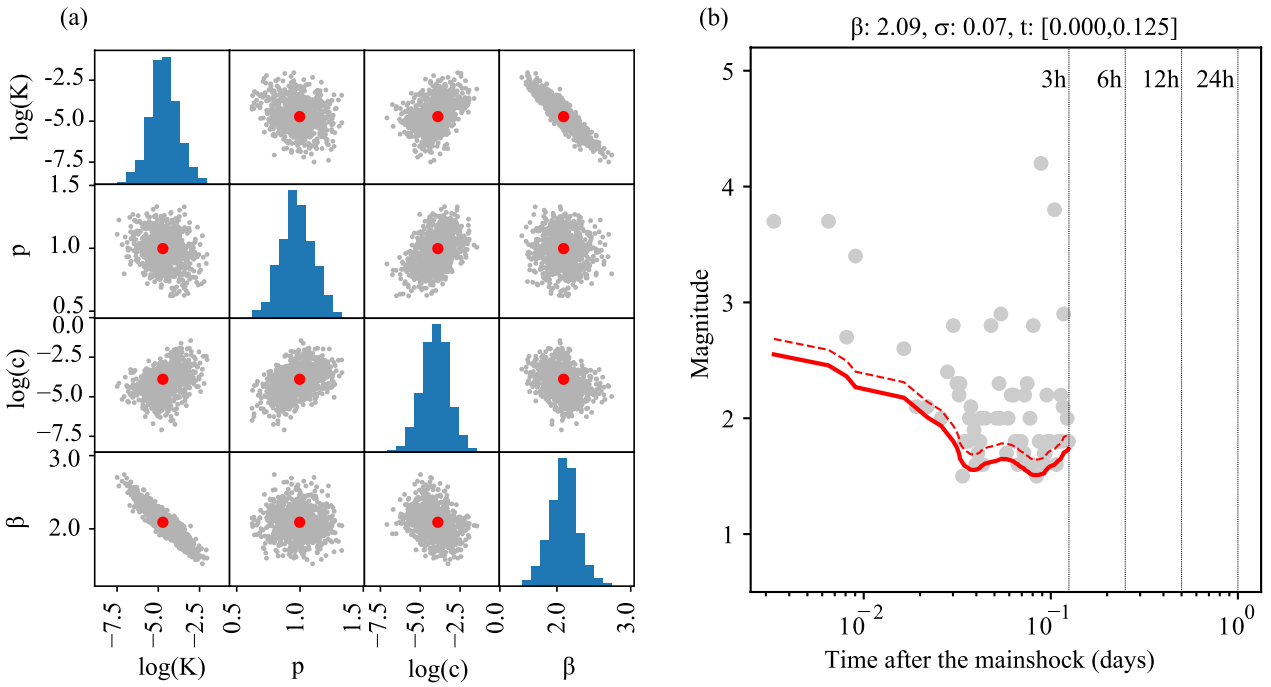

Fig. 6 Estimated parameter sets and evolution of the detection magnitude, $\mu(t)$, and completeness magnitude, $Mc(t)$, for the Gorj sequence (learning period: [0, 3 h] after the mainshock). **a** Scatter plot distributions for the estimated parameter sets for the Gorj sequence (red dots: estimated parameters, gray dots: sampled parameter sets). **b** Evolution of $\mu(t)$ (continuous red line) and $Mc(t)$ (dotted red line) during the learning period

Table 2 Summary of parameter estimations and their uncertainties for the Gorj-Oltenia sequence according to the corresponding learning periods

Learning period, related figures and number of events	*K*	*p*	*c [days]*	*β*	*b*
0–3 h (Figs. 5, 6) (63, 45)	8.89×10^{-3} ($\pm 1.68 \times 10^{-2}$)	1.00 (±0.13)	2.04×10^{-2} ($\pm 2.73 \times 10^{-2}$)	2.09 (±0.21)	0.91 (±0.09)
0–6 h (Figs. S9, S10) (108 70)	1.86×10^{-2} ($\pm 2.51 \times 10^{-2}$)	1.00 (±0.13)	8.06×10^{-2} ($\pm 4.32 \times 10^{-2}$)	2.02 (±0.20)	0.88 (±0.09)
0–9 h (Figs. S11, S12) (142, 77)	2.27×10^{-2} ($\pm 2.20 \times 10^{-2}$)	1.02 (±0.13)	7.59×10^{-2} ($\pm 3.61 \times 10^{-2}$)	1.94 (±0.18)	0.84 (±0.08)
0–12 h (Figs. S13, S14) (178, 62)	2.75×10^{-2} ($\pm 2.06 \times 10^{-2}$)	1.02 (±0.13)	7.95×10^{-2} ($\pm 3.63 \times 10^{-2}$)	1.90 (±0.16)	0.82 (±0.07)
0–24 h (Figs. S15, S16) (240, 174)	9.71×10^{-3} ($\pm 7.04 \times 10^{-3}$)	1.05 (±0.10)	6.55×10^{-2} ($\pm 2.66 \times 10^{-2}$)	2.12 (±0.14)	0.92 (±0.06)

The first column also shows the related figures and the number of events in the learning and forecasting window, respectively

3.3 Aftershock occurrence probability estimations for the two aftershock sequences

In this section, we estimate the probability of aftershocks for both regions, function of magnitude. For our analysis, we chose learning periods of activity after the respective mainshocks of 3 h in Fig. 7, and of 6, 9, 12 and 24 h in Additional File 1—Figures S17–S20. The forecasting was performed for the next 3, 6, 9, 12 and 24 h after the learning periods, respectively.

We found that overall aftershock probabilities were lower for the Marasesti sequence for all forecasting

Table 3 Mean detection magnitudes (μ), standard deviations (σ) and threshold magnitude (M_t) for the Vrancea-Marasesti and Gorj-Oltenia sequences

Seismic sequence	Learning period	μ	σ	M_t (upper rounded M_c at the end of the learning period)
Vrancea-Marasesti	0–3 h	0.45	0.21	0.9
	0–6 h	0.58	0.22	1.1
	0–9 h	0.78	0.21	1.3
	0–12 h	0.71	0.21	1.2
	0–24 h	0.84	0.19	1.3
Gorj-Oltenia	0–3 h	1.73	0.07	1.9
	0–6 h	1.39	0.12	1.7
	0–9 h	1.28	0.11	1.5
	0–12 h	1.16	0.10	1.4
	0–24 h	1.49	0.11	1.8

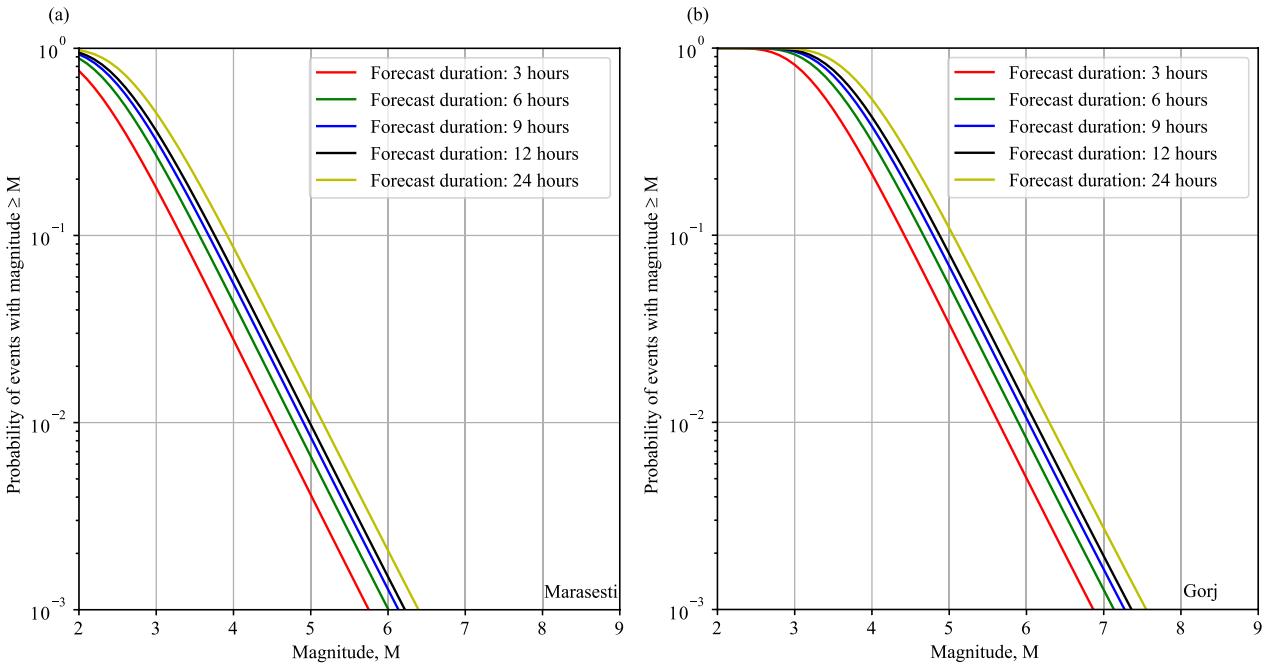

Fig. 7 Aftershock probability forecasts for different forecast windows (of 3, 6, 9, 12 and 24 h) as a function of magnitude. **a** Forecasts for the Marasesti sequence and **b** forecasts for the Gorj sequence, for a learning period of 3 h from the respective mainshocks

periods. Aftershocks of M_L5.7 (i.e., mainshocks magnitudes) or larger in the Marasesti region were forecasted with probabilities of less than 1% (Fig. 7a), while the same magnitudes were determined to have probabilities ranging between 1 and 10% (Fig. 7b) or the Gorj sequence, after the first 3 h from the mainshock.

The results obtained in this study highlight the importance of using real-time forecasting for the Romanian aftershock sequences. Despite having the same mainshock magnitudes, the two sequences evolve rather differently, thus pointing out that a generic model would not be appropriate to characterize and forecast the two sequences.

3.4 Comparison of *b*-values obtained using different methods

As we have discussed previously, the estimation of *b*-values (or β-values; $\beta = b*ln10$) can be significantly biased by the incomplete recording of early aftershocks (e.g., Mignan and Woessner 2012). Here we calculate the β-values and their uncertainties for the Marasesti and Gorj sequences, for the first learning period (0–3 h) using

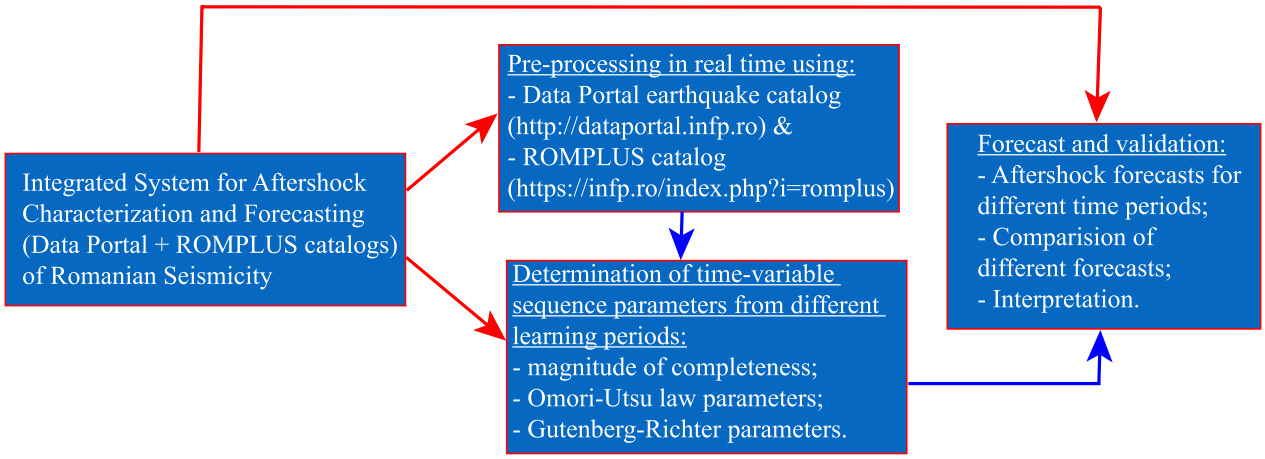

Fig. 8 Integrated system for aftershock characterization and forecasting for Romania

the *b*-positive approach (van der Elst 2021) and compare the results with those determined by our workflow. The *b*-positive method (van der Elst 2021) uses the *b*-positive estimator, which is based on the positive-only subset of the differences in magnitude between successive earthquakes. The estimated β-value and its standard deviation are given by bootstrap (Efron and Tibshirani 1986; Woessner and Wiemer 2005; Petrescu and Enescu 2025). In more detail, 5000 groups of samples (magnitude differences) with the same sample size as that of the original dataset are extracted randomly from the original dataset. The β-values for the 5000 groups of samples are calculated and the obtained average β-value is the estimated β-value, with the standard deviation as the error of the β-value estimation. Increasing the number of groups of samples does not change our conclusions.

Using the procedure outlined above we obtained a β-value of 2.25 ± 0.48, for the Marasesti sequence, and 1.91 ± 0.34, for the Gorj sequence. The corresponding β-values for the two sequences, obtained using our workflow (see Tables 1 and 2, respectively) are 2.03 ± 0.25 and 2.09 ± 0.21, respectively. The β-value obtained for the Marasesti sequence using the *b*-positive approach is larger than that estimated by the workflow, while for the Gorj sequence the opposite can be seen. Nevertheless, for both cases, the two β-values are within their error estimates. Note that the uncertainties for the β-values obtained using the *b*-positive method are larger than those obtained using the workflow method (i.e., the method of Ogata and Katsura (1993), as also reported by Mitsui (2024), since the number of samples of the positive-only subset is smaller than that of the whole data. As also suggested by Mitsui (2024), the two methods should be thoroughly tested and compared in future research. Moreover, the current workflow should be improved by considering β-values (*b*-values) estimated using different approaches.

3.5 The aftershock forecasting system: limitations and future possible developments

Figure 8 shows schematically the concept of our forecasting system for the crustal sequences in Romania. In the present configuration of the system, the Omori–Utsu law is used as a temporal model to issue short-term forecasts immediately after a mainshock. While this simple configuration proves rather robust, it does not capture the secondary or higher-order triggering of aftershocks. To solve this in the future, we will examine the performances of the ETAS model for real-time data and consider replacing the Omori–Utsu modeling with the ETAS model in state-of-the-art implementations (e.g., Petrillo and Zhuang 2024; Mizrahi et al. 2024a, b; Zhang et al. 2024) for longer forecasting periods. We may also consider extending our forecasting model to a space–time model (e.g., Ogata and Zhuang 2006) to provide spatial forecasts.

4 Conclusions

We have proposed for the first time a relatively simple, but robust, analysis and forecasting workflow for the Romanian seismicity, in particular aftershock sequences that occur in crustal regions on the territory of Romania, based on an approach that is currently used for quasi real-time monitoring and forecasting of aftershock sequences in Japan. This approach has been applied to two recent aftershock sequences occurred in 2014 and 2023, in Marasesti and Gorj regions, respectively. Both sequences show a b-value (around 0.8–0.9) of the Gutenberg–Richter law, which is only slightly lower than the average of 1.0 for worldwide seismicity. In both cases the

estimated number of aftershocks, for the chosen forecasting windows, are in general within the estimated uncertainties. We also present probabilities for the occurrence of aftershocks equal or larger than a certain magnitude. Such estimations may help the risk assessment efforts and contribute to better informing the population on future aftershock hazards. Our results are encouraging for the real-time monitoring and forecasting of shallow aftershock sequences in Romania.

Abbreviations

NIEP	National Institute for Earth Physics
ROMPLUS	Romanian earthquake catalogue created and maintained by NIEP
CSCSZ	Central-South Carpathians

Supplementary Information

The online version contains supplementary material available at https://doi.org/10.1186/s40623-025-02174-0.

Additional file 1.

Acknowledgements
We thank our NIEP colleagues for providing the catalog data used in this work and fruitful discussions. We are grateful to Dr. Takahiro Omi for providing his aftershock analysis and forecasting packages and guidance in using his routines. We are grateful to two anonymous reviewers and the Editor, Prof. Zhigang Peng, for insightful comments and suggestions.

Author contributions
Cristian Ghita: data curation, formal analysis, writing—original draft, visualization, data acquisition; Bogdan Enescu: conceptualization, formal analysis, writing—review and editing, supervision, funding acquisition; Alexandru Marinus: formal analysis; Iren-Adelina Moldovan: writing—review and editing, supervision; Constantin Ionescu: supervision; Eduard Gabriel Constantinescu: help with the preparation of map figures. Like An: formal analysis, drawing of some figures. All the authors discussed and approved the final version of this manuscript.

Funding
This research is supported by the JSPS KAKENHI Grant Number JP21H05206 in Transformative Research Areas (A) "Science of Slow to Fast Earthquakes" and the DoGS SPRING Program. It also benefited from funding by the AFROS Project PN-III-P4-ID-PCE-2020-1361, 119 PCE/2021, supported by UEFISCDI, Romania, the NUCLEU Program SOL4RISC, Project no PN23360201, supported by MCID, and PNRR-DTEClimate Project nr. 760008/31.12.2023, Component Project Reactive, supported by Romania—National Recovery and Resilience Plan. The study is also supported by the Ministry of Education, Culture, Sports, Science and Technology (MEXT) of Japan, under its Third Earthquake and Volcano Hazards Observation and Research Program (Earthquake and Volcano Hazard Reduction Research). The funding bodies provided had no specific role in the design of the study and collection, analysis, and interpretation of data and in writing the manuscript should be declared.

Availability of data and materials
The dataportal belongs to the National Seismic Network (RSN) and can be accessed at https://dataportal.infp.ro. The automatic catalog is provided by the National Institute for Earth Physics. The revised ROMPLUS catalog is available at the NIEP website (https://www.infp.ro). They were last accessed on March 31, 2024. We used the following GitHub codes for aftershock forecasting: https://github.com/omitakahiro/AftFore. We also used of the Zmap software (Wiemer 2001) for some of the computations. The inset in Fig. 1 has been obtained by using the GMT software (Wessel et al. 2019). For the Digital Elevation Model (DEM) in Fig. 2, we acknowledge the use of the dataset distributed by the European Space Agency (2024), last accessed on February 21, 2025.

Declarations

Ethics approval and consent to participate
Not applicable.

Consent for publication
Not applicable.

Competing interests
The authors declare that there are no competing interests regarding this manuscript.

Author details
[1]National Institute for Earth Physics, Calugareni Str. 12, P.O. Box MG-2, 077125 Bucharest, Romania. [2]Department of Geophysics, Kyoto University, Kitashirakawa, Oiwake-Cho, Sakyo-Ku, Kyoto 606-8502, Japan.

Received: 30 July 2024 Accepted: 19 March 2025
Published online: 11 April 2025

References

Bala A, Radulian M, Toma-Danila D (2020) Crustal stress partitioning in the complex seismic active areas of Romania. Acta Geod Geoph 55:389–403. https://doi.org/10.1007/s40328-020-00299-0

Cattania C, Werner MJ, Marzocchi W, Hainzl S, Rhoades D, Gerstenberger M, Liukis M, Savran W, Christophersen A, Helmstetter A, Jimenez A, Steacy S, Jordan TH (2018) The forecasting skill of physics-based seismicity models during the 2010–2012 Canterbury, New Zealand, earthquake sequence. Seismol Res Lett 89(4):1238–1250. https://doi.org/10.1785/0220180033

Craiu A, Ghita C, Craiu M, Diaconescu M, Mihai M, Ardeleanu L (2019) The source mechanism of the seismic events during the sequence of the moderate-size crustal earthquake of November 22, 2014 of Vrancea region (Romania). Ann Geophys 61: SE666. https://doi.org/10.4401/ag-7617

Dahm T, Hainzl S (2022) A Coulomb stress response model for time-dependent earthquake forecasts. J Geophys Res Solid Earth 127. https://doi.org/10.1029/2022JB024443

Efron B, Tibshirani R (1986) Bootstrap methods for standard errors, confidence intervals, and other measures of statistical accuracy. Stat Sci 1:54–75. https://doi.org/10.1214/ss/1177013815

Enescu B, Ghita C, Moldovan IA, Radulian M (2023) Revisiting Vrancea (Romania) intermediate-depth seismicity: some statistical characteristics and seismic quiescence testing. Geosciences 13(7):219. https://doi.org/10.3390/geosciences13070219

Enescu B, Mori J, Miyazawa M, Kano Y (2009) Omori-Utsu law c-values associated with recent moderate earthquakes in Japan. Bull Seismol Soc Am 99:884–891. https://doi.org/10.1785/0120080211

European Space Agency (2024) Copernicus global digital elevation model. Distributed by OpenTopography. https://doi.org/10.5069/G9028PQB

Feng Y, Xiong X, Shan B, Liu C (2022) Coulomb stress changes due to the 2021 MS7.4 Maduo earthquake and expected seismicity rate changes in the surroundings. Sci China Earth Sci 65:675–686. https://doi.org/10.1007/s11430-021-9882-8

Fuchs K, Bonjer KP, Bock G, Cornea I, Radu C, Enescu D, Jianu D, Nourescu A, Merkler G, Moldoveanu T, Tudorache G (1979) The Romanian earthquake of March 4, 1977 ii. Aftershocks and migration of seismic activity. Tectonophysics 53(3–4):225–247. https://doi.org/10.1016/0040-1951(79)90068-4

Ghita C, Diaconescu M, Moldovan IA, Oros E, Constantinescu EG (2020) Spatial and temporal variation of seismic b-value beneath Danubian and Hateg-Strei seismogenic areas. Rom Rep Phys 72:704

Ghita C, Diaconescu M, Raicu R, Moldovan IA, Rosu G (2021) The analysis of the seismic sequence started on November 22, 2014 based on ETAS model. Rom Rep Phys 73:708

Godano C, Lippiello E, de Arcangelis L (2014) Variability of the b value in the Gutenberg-Richter distribution. Geophys J Int 199(3):1765–1771. https://doi.org/10.1093/gji/ggu359

Gutenberg B, Richter CF (1944) Frequency of earthquakes in California. Bull Seismol Soc Am 34:185–188. https://doi.org/10.1785/BSSA0340040185
Hardebeck JL, Llenos AL, Michael AL, Page MT, Schneider M, van der Elst NJ (2024) Aftershock forecasting. Ann Rev Earth Planet Sci 52:61–84. https://doi.org/10.1146/annurev-earth-040522-102129
Jia K (2020) Modeling the spatiotemporal seismicity patterns of the Longmen Shan Fault Zone based on the Coulomb rate and state model. Seismol Res Lett 92:275–286. https://doi.org/10.1785/0220200088
Kagan YY (2004) Short-term properties of earthquake catalogs and models of earthquake source. Bull Seismol Soc Am 94:1207–1228. https://doi.org/10.1785/012003098
Lippiello E, Petrillo G (2024) b-more-incomplete and b-more-positive: insights on a robust estimator of magnitude distribution. J Geophys Res Solid Earth 129. https://doi.org/10.1029/2023JB027849
Mancini S, Segou M, Werner MJ, Parsons T, Beroza G, Chiaraluce L (2022) On the use of high-resolution and deep-learning seismic catalogs for short-term earthquake forecasts: potential benefits and current limitations. J Geophys Res Solid Earth 127. https://doi.org/10.1029/2022JB025202
Marmureanu A, Ionescu C, Grecu B, Toma-Danila D, Tiganescu A, Neagoe C, Toader V, Craifaleanu IG, Dragomir CS, Meita V, Liashchuk A, Dimitrova L, Ilies I (2021) From national to transnational seismic monitoring products and services in the Republic of Bulgaria, Republic of Moldova, Romania, and Ukraine. Seismol Res Lett 92:1685–1703. https://doi.org/10.1785/0220200393
Mignan A, Woessner J (2012) Estimating the magnitude of completeness for earthquake catalogs. Commun Online Resour Stat Seism Anal. https://doi.org/10.5078/corssa-00180805
Mizrahi L, Dallo I, van der Elst NJ, Christophersen A, Spassiani I, Werner M, Iturrieta P. Bayona JA, Iervolino I, Schneider M, Page MT, Zhuang J, Herrmann M, Michael AJ, Falcone G, Marzocchi W, Rhoades D, Gerstenberger M, Gulia L, Schorlemmer D, Becker J, Han, Marta, Kuratle L, Marti M, Wiemer S (2024) Developing, testing, and communicating earthquake forecasts: current practices and an elicitation of expert recommendations. Rev Geophys 62. https://doi.org/10.1029/2023RG000823
Mizrahi L, Nandan S, Cabrera BM, Wiemer S (2024b) suiETAS: developing and testing ETAS-based earthquake forecasting models for Switzerland. Bull Seismol Soc Am 114(5):2591–2612. https://doi.org/10.1785/0120240007
Moldovan IA, Popescu E, Constantin A (2008) Probabilistic seismic hazard assessment in Romania: application for crustal seismic active zones. Rom J Phys 53(3–4):575–591
Morikawa K, Nagao H, Ito S, Terada Y, Sakai S, Hirata N (2021) Forecasting temporal variation of aftershocks immediately after a main shock using Gaussian process regression. Geophys J Int 226(2):1018–1035. https://doi.org/10.1093/gji/ggab124
Nandan S, Ouillon G, Sornette D, Wiemer S (2019) Forecasting the rates of future aftershocks of all generations is essential to develop better earthquake forecast models. J Geophys Res 124:8404–8425. https://doi.org/10.1029/2018JB016668
Nomura S, Ogata Y, Komaki F, Toda S (2011) Bayesian forecasting of recurrent earthquakes and predictive performance for a small sample size. J Geophys Res 116:B04315. https://doi.org/10.1029/2010JB007917
Ogata Y, Katsura K (1993) Analysis of temporal and spatial heterogeneity of magnitude frequency distribution inferred from earthquake catalogues. Geophys J Int 113:727–738. https://doi.org/10.1111/j.1365-246X.1993.tb04663.x
Ogata Y, Katsura K (2006) Immediate and updated forecasting of aftershock hazard. Geophys Res Lett 33:L10305. https://doi.org/10.1029/2006GL025888
Ogata Y, Zhuang J (2006) Space–time ETAS models and an improved extension. Tectonophysics 413(1–2):13–23. https://doi.org/10.1016/j.tecto.2005.10.016
Omi T, Ogata Y, Hirata Y, Aihara K (2013) Forecasting large aftershocks within one day after the main shock. Sci Rep 3:2218. https://doi.org/10.1038/srep02218
Omi T, Ogata Y, Hirata Y, Aihara K (2014) Estimating the ETAS model from an early aftershock sequence. Geophys Res Lett 41:850–857. https://doi.org/10.1002/2013GL058958
Omi T, Ogata Y, Hirata Y, Aihara K (2015) Intermediate-term forecasting of aftershocks from an early aftershock sequence: Bayesian and ensemble forecasting approaches. J Geophys Res 120:2561–2578. https://doi.org/10.1002/2014JB011456
Omi T, Ogata Y, Shiomi K, Enescu B, Sawazaki K, Aihara K (2016) Automatic aftershock forecasting: a test using real-time seismicity data in Japan. Bull Seismol Soc Am 106:2450–2458. https://doi.org/10.1785/0120160100
Omi T, Ogata Y, Shiomi K, Enescu B, Sawazaki K, Aihara K (2019) Implementation of a real-time system for automatic aftershock forecasting in Japan. Seismol Res Lett 90:242–250. https://doi.org/10.1785/0220180213
Oncescu MC, Marza VI, Rizescu M, Popa M (1999) The Romanian earthquake catalogue between 984–1997. In: Wenzel F, Lungu D, Novak O (eds) Vrancea earthquakes: tectonics, hazard and risk mitigation. Advances in natural and technological hazards research, vol 11. Springer, Dordrecht, pp 43–47. https://doi.org/10.1007/978-94-011-4748-4_4
Oros E, Popa M, Paulescu D, Placinta AO, Ghita C (2023) A refined catalogue of focal mechanisms for the Intra-Carpathian region of Romania: implications for the stress field and seismogenic features assessment. Ann Geophys 65: SE639. https://doi.org/10.4401/ag-8387.
Page MT, van der Elst N, Hardebeck J, Felzer K, Michael AJ (2016) Three ingredients for improved global aftershock forecasts: tectonic region, time-dependent catalog incompleteness, and intersequence variability. Bull Seismol Soc Am 106:2290–2301. https://doi.org/10.1785/0120160073
Pavel F (2017) Next future large earthquake in Romania: a disaster waiting to happen? Seismol Res Lett 88(1):1–3. https://doi.org/10.1785/022016014
Peng Z, Vidale JE, Ishii M, Helmstetter A (2007) Seismicity rate immediately before and after main shock rupture from high-frequency waveforms in Japan. J Geophys Res 112:B03306. https://doi.org/10.1029/2006JB004386
Peng Z, Zhao P (2009) Migration of early aftershocks following the 2004 Parkfield earthquake. Nat Geosci 2:877–881. https://doi.org/10.1038/ngeo697
Petrescu L, Enescu B (2025) Seismicity of a relic slab: space–time cluster analysis in the Vrancea seismic zone. Earth Planets Sp 77:6. https://doi.org/10.1186/s40623-025-02136-6
Petrillo G, Zhuang J (2024) Bayesian earthquake forecasting approach based on the epidemic type aftershock sequence model. Earth Planet Sp 76:78. https://doi.org/10.1186/s40623-024-02021-8
Placinta AO, Popescu E, Borleanu F, Radulian M, Popa M (2016) Analysis of source properties for the earthquake sequences in the South-Western Carpathians (Romania). Rom Rep Phys 68:1240–1258
Popa M, Chircea A, Dinescu R, Neagoe C, Grecu B, Borleanu F (2022) Romanian earthquake catalogue (ROMPLUS). Mendeley Data 2022 V2. https://doi.org/10.17632/tdfb4fgghy.2
Popa M, Radulian M, Ghica D, Neagoe C, Nastase E (2015). Romanian seismic network since 1980 to the present. In: Aneva B, Kouteva-Guentcheva M (eds) Nonlinear mathematical physics and natural hazards, Springer proceedings in physics vol 163. Springer, Cham, pp 117–131. https://doi.org/10.1007/978-3-319-14328-6_9
Popescu E, Borleanu F, Rogozea M, Radulian M (2012) Source analysis for earthquake sequence occurred in Vrancea (Romania) region on 6 to 30 September 2008. Rom Rep Phys 64:571–590
Popescu E, Neagoe C, Rogozea M, Moldovan IA, Borleanu F, Radulian M (2011) Source parameters for the earthquake sequence occurred in the Ramnicu Sarat area (Romania) in November–December 2007. Rom J Phys 56:265–278
Popescu E, Radulian M (2001) Source characteristics of the seismic sequences in the Eastern Carpathians foredeep region (Romania). Tectonophysics 338:325–337. https://doi.org/10.1016/S0040-1951(01)00087-7
Radulian M, Popescu E, Borleanu F, Diaconescu M (2014) Source parameters of the December 2011–January 2012 earthquake sequence in Southern Carpathians, Romania. Tectonophysics 623:23–38. https://doi.org/10.1016/j.tecto.2014.03.014
Reasenberg PA, Jones LM (1989) Earthquake hazard after a mainshock in California. Science 243:1173–1176
Savran WH, Werner MJ, Marzocchi W, Rhoades DA, Jackson DD, Milner K, Field E, Michael A (2020) Pseudoprospective evaluation of UCERF3-ETAS forecasts during the 2019 Ridgecrest sequence. Bull Seismol Soc Am 110(4):1799–1817. https://doi.org/10.1785/0120200026
Scholz CH (2015) On the stress dependence of the earthquake b value. Geophys Res Lett 42:1399–1402. https://doi.org/10.1002/2014GL062863

Seghedi A, Vaida M, Iordan M, Verniers J (2005) Paleozoic evolution of the Romanian part of the Moesian platform: an overview. Geol Belg 8:99–120
Shimojo K, Enescu B, Yagi Y, Takeda T (2021) Nucleation process of the 2011 northern Nagano earthquake from nearby seismic observations. Sci Rep 11:8143. https://doi.org/10.1038/s41598-021-86837-4
Toda S, Enescu B (2011) Rate/state Coulomb stress transfer model for the CSEP Japan seismicity forecast. Earth Planet Sp 63:171–185. https://doi.org/10.5047/eps.2011.01.004
Tormann T, Enescu B, Woessner J, Wiemer S (2015) Randomness of megathrust earthquakes implied by rapid stress recovery after the Japan earthquake. Nat Geosci 8:152–158. https://doi.org/10.1038/ngeo2343
Utsu T (1961) A statistical study on the occurrence of aftershocks. Geophys Mag 30:521–605. https://doi.org/10.4401/ag-5094
Utsu T (1970) Aftershocks and earthquake statistics (2): further investigation of aftershocks and other earthquake sequences based on a new classification of earthquake sequences. J Fac Sci Hokkaido Univ Ser VII (Geophysics) 3:197–266
Utsu T, Ogata Y, Matsu'ura RS (1995) The centenary of the Omori formula for a decay law of aftershock activity. J Phys Earth 43:1–33. https://doi.org/10.4294/jpe1952.43.1
van der Elst NJ (2021) B-positive: a robust estimator of aftershock magnitude distribution in transiently incomplete catalogs. J Geophys Res Solid Earth 126. https://doi.org/10.1029/2020JB021027
van der Elst NJ, Hardebeck, JL, Michael AJ, McBride SK, Vanacore E (2022) Prospective and retrospective evaluation of the U.S. geological survey public aftershock forecast for the 2019–2021 Southwest Puerto Rico earthquake and aftershocks. Seismol Res Lett 93(2A):620–640. https://doi.org/10.1785/0220210222
Wessel P, Luis JF, Uieda L, Scharroo R, Wobbe F, Smith WHF, Tian D (2019) The generic mapping tools version 6. Geochem Geophys Geosyst 20(11):5556–5564. https://doi.org/10.1029/2019GC008515
Wiemer S (2001) A software package to analyze seismicity: ZMAP. Seismol Res Lett 72:373–382. https://doi.org/10.1785/gssrl.72.3.373
Woessner J, Wiemer S (2005) Assessing the quality of earthquake catalogues: estimating the magnitude of completeness and its uncertainty. Bull Seismol Soc Am 95(2):684–698. https://doi.org/10.1785/0120040007
Zhang H, Ke S, Liu W, Zhang Y (2024) A combining earthquake forecasting model between deep learning and epidemic-type aftershock sequence (ETAS) model. Geophys J Int 239(3):1545–1556. https://doi.org/10.1093/gji/ggae349
Zhuang J (2011) Next-day earthquake forecasts for the Japan region generated by the ETAS model. Earth Planet Sp 63:207–216. https://doi.org/10.5047/eps.2010.12.010

Publisher's Note